

Leggett-Garg violations for continuous variable systems with gaussian states

C. Mawby* and J.J.Halliwell†

Blackett Laboratory

Imperial College

London SW7 2BZ

UK

Abstract

Macrorealism (MR) is the world view that certain quantities may take definite values at all times irrespective of past or future measurements and may be experimentally falsified via the Leggett-Garg (LG) inequalities. We put this world view to the test for systems described by a continuous variable x by seeking LG violations for measurements of a dichotomic variable $Q = \text{sign}(x)$, in the case of gaussian initial states in a quantum harmonic oscillator. Extending our earlier analysis [C. Mawby and J. J. Halliwell, Phys. Rev. A **105**, 022221 (2022)] we find analytic expressions for the temporal correlators. An exploration of parameter space reveals significant regimes in which the two-time LG inequalities are violated, and likewise at three and four times. To obtain a physical picture of the LG violations, we exploit the continuous nature of the underlying position variable and analyse the relevant quantum-mechanical currents, Bohm trajectories, and Wigner function. Further, we extend the analysis LG tests using coherent state projectors, thermal coherent states, and squeezed states.

*Electronic address: c.mawby18@imperial.ac.uk

†Electronic address: j.halliwell@imperial.ac.uk

1. INTRODUCTION

The motion of a pendulum has been used by clockmakers and hypnotists alike for centuries, with its regular left, right, left motion. Scaled down enough, the quantum mechanical description becomes necessary, which hints that non-classical states without a definite left-right property underlie the motion. The existence of these type of states form one of the pillars of many quantum technologies, and hence verification of their existence, and an understanding of their persistence to macroscopic scales is of great interest.

The Leggett-Garg inequalities [1–4] were introduced to provide a quantitative test capable of demonstrating the failure of the precise world view known as macrorealism (MR). MR is defined as the conjunction of three realist tenets – that a system resides in one observable state only, for all instants of time, which may be measured without influencing future dynamics of the system, and that measurements respect causality. The violation of these inequalities indicates a failure of MR, and hence the presence of non-classical behaviour.

The LG inequalities are typically established for a dichotomic observable Q , which may take value $s_i = \pm 1$, measured in a series of experiments at single times and at pairs of times. This yields a data set consisting of single time averages $\langle Q_i \rangle$, where $Q_i = Q(t_i)$, and the temporal correlators C_{ij} defined by

$$C_{ij} = \langle Q_i Q_j \rangle = \sum_{s_i, s_j} s_i s_j p(s_i, s_j), \quad (1.1)$$

where $p(s_i, s_j)$ is the two-time measurement probability, giving the likelihood of measuring s_i and s_j at times t_i, t_j . The temporal correlators must be measured in a non-invasive manner, in keeping with the definition of MR, which is typically done using ideal negative measurements [5–7] (but other approaches exist [8–10]).

For the commonly-studied three time case, the data set consists of three correlators C_{12}, C_{23}, C_{13} and three single time averages $\langle Q_i \rangle$, $i = 1, 2, 3$. These quantities then form six puzzle-pieces that, should the system obey the assumptions of MR, must be the moments of an underlying joint probability distribution $p(s_1, s_2, s_3)$. In the case where this endeavour

is possible, the correlators and averages will satisfy the three-time LG inequalities (LG3):

$$L_1 = 1 + C_{12} + C_{23} + C_{13} \geq 0, \quad (1.2)$$

$$L_2 = 1 - C_{12} - C_{23} + C_{13} \geq 0, \quad (1.3)$$

$$L_3 = 1 + C_{12} - C_{23} - C_{13} \geq 0, \quad (1.4)$$

$$L_4 = 1 - C_{12} + C_{23} - C_{13} \geq 0. \quad (1.5)$$

They will also satisfy a set of twelve two-time LG inequalities (LG2), four of which are of the form,

$$1 + s_1 \langle Q_1 \rangle + s_2 \langle Q_2 \rangle + s_1 s_2 C_{12} \geq 0 \quad (1.6)$$

where $s_1, s_2 = \pm 1$, with two more sets of four for the other two time pairs. This set of sixteen inequalities are necessary and sufficient conditions for MR [11–16]. If any one of them is violated, MR fails. From an experimental point of view, the LG2 inequalities constitute the simplest place to look first, since only one correlator needs to be measured.

For measurements at four times, there are six correlators, but the natural data set is a cycle of four $C_{12}, C_{23}, C_{34}, C_{14}$, along with the four single time averages. The LG4 inequalities take the form

$$-2 \leq C_{12} + C_{23} + C_{34} - C_{14} \leq 2, \quad (1.7)$$

together with the six more inequalities permuting the location of the minus sign. The necessary and sufficient conditions for MR at four times consist of these eight LG4 inequalities, together with the set of sixteen LG2s for the four time pairs [11–14].

This general framework has been put to the test experimentally in many types of systems. See for example Refs. [5–7, 9, 17–19] and also the useful review [4]. Most of these experiments are on systems that are essentially microscopic but some come close to macroscopicity [20]. Note also the useful critique of the LG approach Ref. [21].

In the present paper we investigate LG tests for the quantum harmonic oscillator. The LG framework is readily adapted to this physical situation using a single dichotomic variable $Q = \text{sgn}(x)$, where x is the particle position, measured at different times. We build on our earlier work Ref. [22], which explored LG violations in the QHO for initial states consisting of harmonic oscillator eigenstates and superpositions thereof, finding close to maximal violations in some cases. Here we focus on the case of an initial coherent state and closely related states. Such an initial state is intriguing in this context since it is often regarded as

essentially classical, being a phase space localized state evolving along a classical trajectory. Hence any LG violations arising from this state constitute particularly striking examples of non-classical behaviour.

LG tests for the QHO with an initial coherent state were first explored by Bose et al [23], who proposed an experiment to measure the temporal correlators and carried out calculations of LG4 violations. A subsequent paper [24] explored both LG2 violations and also violations of the no-signalling in time conditions [25–27]. Our work in part parallels Ref. [24].

The first main aim of this paper is to undertake a thorough analysis of LG2, LG3 and LG4 inequalities for an initial coherent state. This is carried out in Section 2, where we set out the formalism, drawing on our earlier work [22], and in Section 3, where we carry out a detailed parameter search and find the largest LG violations possible for a coherent state.

A second aim is to explore the physical origins of the LG violations. So, in Section 4 we examine the difference between quantum-mechanical currents and their classical counterparts for initial coherent states projected onto the positive or negative x -axis, and we also illustrate the results using Bohm trajectories. Also, in Section 5, we examine the measurement process in the Wigner representation, noting that the initially positive Wigner function of the coherent state acquires negativity as a result of the projective measurement process.

Modifications to the above framework are considered in Sections 6 and 7. In Section 6 we briefly discuss other types of measurements beyond the simple projective position measurements used so far and also consider LG2 violations with projections onto coherent states. In Section 7, we consider how the LG violations may be modified for squeezed states or thermal states. We summarize in Section 8.

2. TEMPORAL CORRELATORS FOR COHERENT STATES

A. Conventions and Strategy

For most of this paper, we will work with coherent states of the harmonic potential, which can of course be thought of as the ground state of the QHO, shifted in phase-space. The intricacy of calculating temporal correlators within QM stems from the complexity in

the time evolution of a post-measurement state. By considering a co-moving frame for the post-measurement state, we develop a time evolution result which explicitly separates the quantum behaviour from the classical trajectories.

We will work with systems defined exactly (or approximately) by the harmonic oscillator Hamiltonian,

$$\hat{H} = \frac{\hat{p}_{\text{phys}}^2}{2m} + \frac{1}{2}m\omega^2\hat{x}_{\text{phys}}^2, \quad (2.1)$$

with physical position and momenta x_{phys} and p_{phys} . In calculations we use the standard dimensionless variables $x\sqrt{\hbar/(m\omega)} = x_{\text{phys}}$ and $p\sqrt{\hbar m\omega} = p_{\text{phys}}$. We denote energy eigenstates $|n\rangle$, represented in the position basis $\psi_n(x) = \langle x|n\rangle$, with corresponding energies $E_n = \hbar\omega(n + \frac{1}{2}) = \varepsilon_n\hbar\omega$.

We write coherent states as $|\alpha\rangle$, where its eigenvalue α relates to rescaled variables as

$$\langle \hat{x}(t) \rangle = \sqrt{2} \text{Re } \alpha(t), \quad (2.2)$$

$$\langle \hat{p}(t) \rangle = \sqrt{2} \text{Im } \alpha(t). \quad (2.3)$$

These are the classical paths underlying the motion of coherent states, and we adopt the short-hand $x_1 = \langle \hat{x}(t_1) \rangle$ and likewise $p_1 = \langle \hat{p}(t_1) \rangle$. A coherent state may be represented in terms of α and an initial phase, however in this work we will largely represent them in terms of the initial averages x_0 and p_0 , for clarity of physical understanding. We construct coherent states with the unitary displacement operator $D(\alpha) = \exp(\alpha\hat{a}^\dagger - \alpha^*\hat{a})$ operating on the ground state,

$$|\alpha\rangle = D(\alpha) |0\rangle, \quad (2.4)$$

which results in the wave-function

$$\psi^\alpha(x, t) = \frac{1}{\pi^{1/4}} \exp\left(-\frac{1}{2}(x - x_t)^2 + i\frac{p_t}{\hbar}x + i\gamma(t)\right). \quad (2.5)$$

We will calculate the quantities $\langle Q_i \rangle$, C_{ij} appearing in the LG inequalities. A convenient way to proceed is to first note that the combination appearing in the LG2 inequalities is proportional to the quantity

$$q(s_1, s_2) = \frac{1}{4} \left(1 + s_1 \langle \hat{Q}_1 \rangle + s_2 \langle \hat{Q}_2 \rangle + s_1 s_2 C_{12} \right). \quad (2.6)$$

Classically this quantity is non-negative and is the probability distribution matching the data set with moments of $\langle Q_1 \rangle$, $\langle Q_2 \rangle$, C_{12} . In the quantum-mechanical case, this quantity

may be written

$$q(s_1, s_2) = \text{ReTr}(P_{s_2}(t_2)P_{s_1}(t_1)\rho), \quad (2.7)$$

where $s = \pm 1$, and P_s are projection operators corresponding to the measurement made, with

$$P_s = \frac{1}{2}(1 + s\hat{Q}). \quad (2.8)$$

Since Eq. (2.7) can be negative (up to a maximum of $-\frac{1}{8}$), it is referred to as a quasi-probability (QP) [11, 28]. Purely from a calculational point of view it is a convenient object to work with, as we found in Ref. [22], since it is proportional to the LG2 inequalities in the quantum case, and since the correlators are easily read off from its moment expansion, so we make use of it here.

B. Correlators for left-right measurements

The quasi-probability for coherent states with the left-right dichotomic variable, $P_s = \theta(s\hat{x})$, is given by

$$q(s_1, s_2) = \text{Re} \langle \alpha | e^{\frac{iHt_2}{\hbar}} \theta(s_2\hat{x}) e^{-\frac{iH\tau}{\hbar}} \theta(s_1\hat{x}) e^{-\frac{iHt_1}{\hbar}} | \alpha \rangle. \quad (2.9)$$

By considering the displacement operator as acting on the measurements instead of the state, the quasi-probability is shown in Appendix A to be

$$q(s_1, s_2) = \text{Re} e^{\frac{i\omega\tau}{2}} \langle 0 | \theta(s_2(\hat{x} + x_2)) e^{-iH\tau} \theta(s_1(\hat{x} + x_1)) | 0 \rangle, \quad (2.10)$$

which reveals that the quasi-probability for coherent states can be understood as the quasi-probability for the pure ground state, with measurement profiles translated according to the classical paths.

A calculation similar to that in our earlier paper Ref. [22] shows the quasi-probability is

$$q(+, +) = \text{Re} e^{\frac{i\omega\tau}{2}} \sum_{n=0}^{\infty} e^{-i\omega\tau(n+\frac{1}{2})} \langle 0 | \theta(\hat{x} + x_2) | n \rangle \langle n | \theta(\hat{x} + x_1) | 0 \rangle, \quad (2.11)$$

and similarly for the other three components. The matrix elements here are given by the J_{mn} matrices from our earlier paper [22, 29],

$$J_{mn}(x_1, x_2) = \int_{x_1}^{x_2} dx \langle m | x \rangle \langle x | n \rangle. \quad (2.12)$$

The quasi-probability is then

$$q(+, +) = \text{Re} \sum_{n=0}^{\infty} e^{-in\omega\tau} J_{0n}(x_1, \infty) J_{0n}(x_2, \infty) \quad (2.13)$$

For $m \neq n$, the J matrices take the value

$$J_{mn}(x_1, x_2) = \frac{1}{2(\varepsilon_n - \varepsilon_m)} [\psi'_m(x_2)\psi_n(x_2) - \psi'_n(x_2)\psi_m(x_2) - \psi'_m(x_1)\psi_n(x_1) + \psi'_n(x_1)\psi_m(x_1)], \quad (2.14)$$

where $\psi_n(x) = \langle x|n \rangle$. For the $n = m = 0$ case, the integration is completed manually yielding

$$J_{00}(x, \infty) = \frac{1}{2}(1 - \text{erf}(x)). \quad (2.15)$$

Hence writing out the quasi-probability with $n = 0$ case of the sum handled, we have

$$q(s_1, s_2) = \frac{1}{4} \left[1 + s_1 \text{erf}(x_1) + s_2 \text{erf}(x_2) + s_1 s_2 \left(\text{erf}(x_1) \text{erf}(x_2) + 4 \text{Re} \sum_{n=1}^{\infty} e^{-in\omega\tau} J_{0n}(x_1, \infty) J_{0n}(x_2, \infty) \right) \right]. \quad (2.16)$$

Comparing to the moment expansion of the quasi-probability, we obtain the correlators

$$C_{12} = \text{erf}(x_1) \text{erf}(x_2) + 4 \text{Re} \sum_{n=1}^{\infty} e^{-in\omega\tau} J_{0n}(x_1, \infty) J_{0n}(x_2, \infty). \quad (2.17)$$

The infinite sum may be evaluated approximately using numerical methods, by summing up to a finite n . This calculation matches the analytically calculated special case of $x_0 = 0$ given in Ref. [30].

It is easily seen that the quasi-probability Eq. (2.16) is non-negative if the infinite sum vanishes. This means the infinite sum is the only source of negativity.

We now observe that the J_{0n} terms in the infinite sum will be suppressed if either $|x_1|$ or $|x_2|$ become large, since each term involves a factor of either $\psi_0(x)$ or $\psi'_0(x)$, resulting in double-exponential suppression. We can place a limit on the magnitude of the sum in Eq.(2.16), by considering it as the overlap between $\theta(x - x_1)\psi_0(x)$ and $\theta(x - x_2)\psi_0(x)$, less $J_{00}(x_1, \infty)J_{00}(x_2, \infty)$. This yields the limit

$$\left| \sum_{n=1}^{\infty} e^{-in\omega\tau} J_{0n}(x_1, \infty) J_{0n}(x_2, \infty) \right| \leq \frac{1}{2} \theta(x_1 - x_2) (\text{erf}(x_2) + \text{erfc}(x_1) - 1) - \frac{1}{4} (\text{erfc}(x_1) - 2) \text{erfc}(x_2). \quad (2.18)$$

A quick evaluation shows that with either $|x_1|$ or $|x_2|$ greater than 3, the magnitude of the sum is limited to the order of 10^{-6} . This means that if the coherent state is a significant distance from the axis at either of the measurement times, the sum containing the quantum effects will vanish, and the quasi-probability will be non-negative.

The same applies to the correlators Eq. (2.17) used in the LG inequalities, where any $x_i > 3$ renders the correlators involving that measurement time classical. This does not rule out the possibility of LG3/4 violations with $x_i > 3$, but it does mean at least two of the correlators will be forced to be classical, which will clearly reduce in magnitude any possible violations.

Altogether this corresponds to the requirement that each measurement must make a significant chop of the state, which fits the intuition that without significant chopping, there is no mystery attached to which side of the axis the particle may be found on.

3. LG VIOLATIONS WITH PROJECTIVE MEASUREMENTS

In this section, we explore the behaviour of the LG inequalities for coherent states. The quantities appearing in the LG inequalities depend on the initial position and momentum of the coherent state and the time intervals between measurements. We take all time intervals to be the same and equal to τ , resulting in a three-dimensional parameter space.

We also note, that it is sufficient to explore a single quadrant of the x_0, p_0 parameter space, which we take to be the positive quadrant. For states with $x_0 < 0$, the quasi-probability may be recovered by inverting the sign of s_1 . Likewise for states with $p_0 < 0$, by allowing the interval between measurements to take values $0 < \tau \leq 2\pi$, their behaviour is included in the positive quadrant. This same argument applies to the LG inequalities in general, where their different permutations correspond to flips of measurement signs.

To represent the three-dimensional parameter space, for each x_0, p_0 , we use numerical minimisation over $0 < \tau \leq 2\pi$ to find the largest possible violation for that coherent state. In this numerical procedure, we take the largest possible violation from all of the inequalities involved.

In Fig. 1(a), we plot the parameter space for the LG2 inequalities Eq. (1.6). We reach a largest violation of -0.0113 , which represents 22% of the maximal violation possible. We note that the largest violations occur with the initial state off-set from the center of the well,

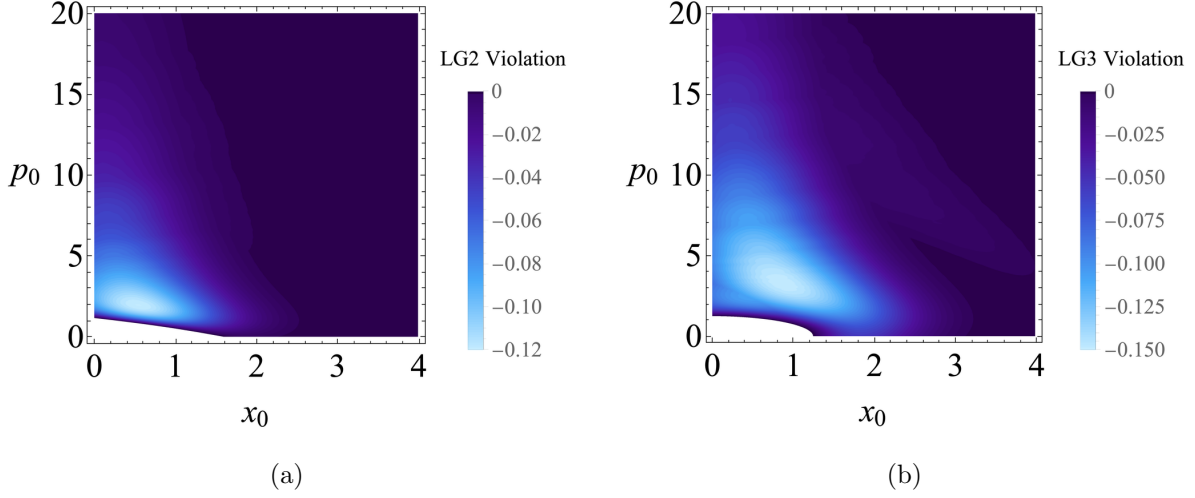


FIG. 1: Plot (a) shows the greatest possible violations for the LG2 inequalities, plot (b) shows the same for the LG3 inequalities.

centred around $|x_0| = 0.55$, and $|p_0| = 1.925$.

In Fig. 1(b), the parameter space for the LG3 inequalities Eqs. (1.2)-(1.5) is plotted. Here a largest violation of -0.141 is found, which represents 28% of the maximal possible violation. The regions of violation for the LG3 inequalities occurs over a large range of x_0 , and extends further to higher momenta as well. We find maximal violation centered around $|x_0| = 0.859$, $|p_0| = 3.32$.

In Fig. 2, we plot the parameter space for the LG4 inequalities Eq. (1.7). We find a largest violation of 2.21, representing 26% of the maximal violation for LG4 inequalities. The region of violation is broader again than the LG3s, with maximal violations centered around $|x_0| = 0.93$, $|p_0| = 3.66$.

We note that common to all of these inequalities is the quarter-circle at the centre. This is the set of states close to the ground state $|0\rangle$, for which we know from Ref. [22] there are no LG violations. Outside of this circle, the plots reveals that the most significant LG violations are found at lower momenta. Both the magnitude and quantity of violations decrease as momentum increases. We tabulate these results in Table I.

In Figures 3, 4 and 5, we plot the temporal behaviour of the LG2s, LG3s and LG4s respectively, for the case in which the parameters are chosen to give the largest violation.

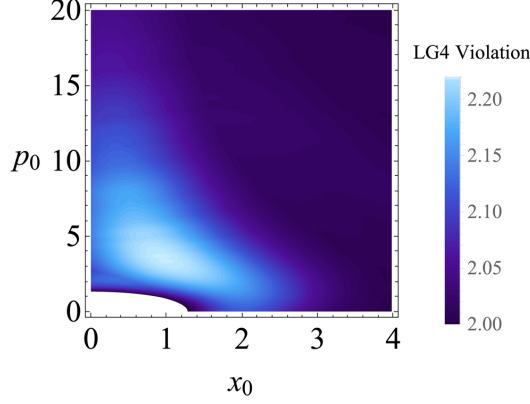


FIG. 2: The largest LG4 violations for coherent states with initial parameters x_0, p_0 .

4. MECHANISMS OF VIOLATION

Given the LG violations exhibited in the previous section a natural question to ask concerns the underlying physical effects producing the non-classical behaviour responsible for the violations. Since $Q(t) = \text{sgn}(x(t))$, a classical picture of the system would involve a set of trajectories $x(t)$ and probabilities for those trajectories. It is then natural to look at the parallel structures in quantum theory and compare with the classical analogues. We therefore look at the quantum-mechanical currents associated with the LG inequalities, which correspond to the time evolution of certain probabilities, and also to the Bohm trajectories associated with those currents, in terms of which the probability flow in space-time is easily seen. What we will see is that the departures from classicality are essentially the “diffraction in time” effect first investigated by Moshinsky, who considered the time evolution of an initial plane wave in one dimension restricted to $x < 0$ [31, 32]. The key mathematical object is the Moshinsky function

$$M(x, p, t) = \langle x | e^{-iHt} \theta(\hat{x}) | p \rangle \quad (4.1)$$

Inequality	Largest Violation	Percent of Maximal	Location ($ x_0 , p_0 $)
LG2	-0.113	22%	(0.550, 1.925)
LG3	-0.141	28%	(0.859, 3.317)
LG4	2.216	26%	(0.929, 3.666)

TABLE I: Tabulation of parameter space results.

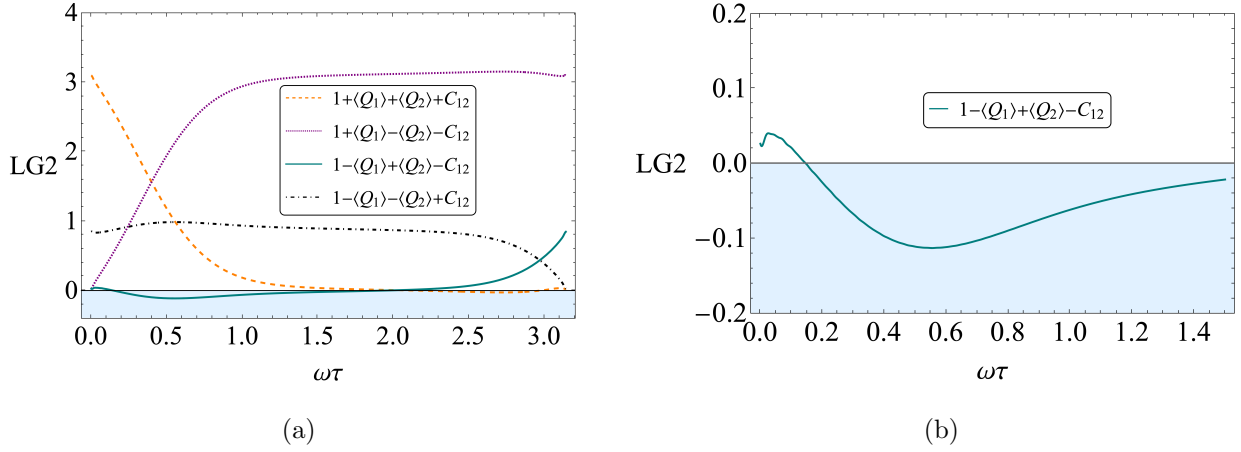


FIG. 3: Plot (a) shows the four LG2 inequalities for the state with $x_0 = 0.55$, $p_0 = -1.925$, which reaches a largest negativity of -0.113 . Plot (b) shows a zoom of the violated inequality for this state.

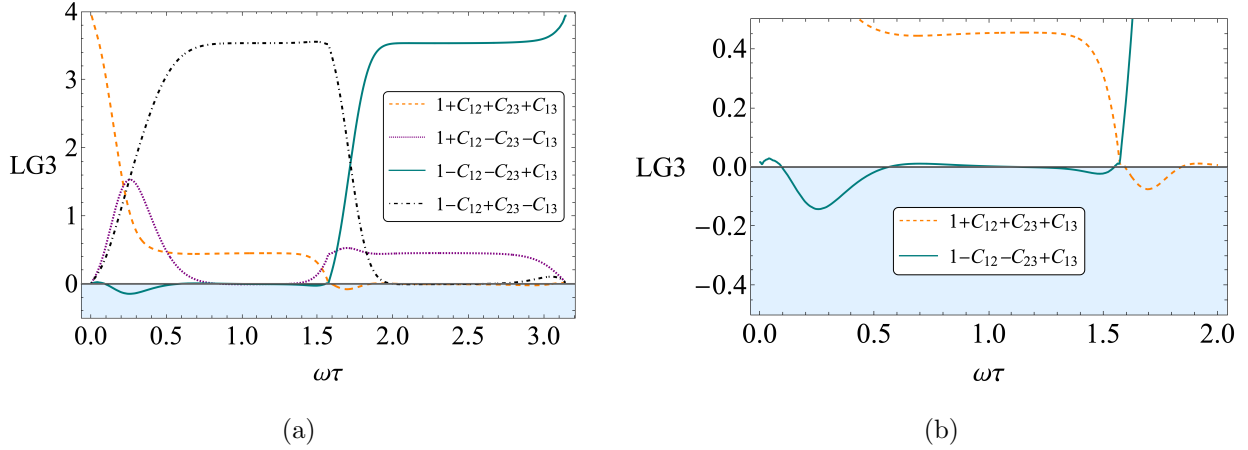


FIG. 4: Plot (a) shows the four LG3 inequalities for the state with $x_0 = 0.859$, $p_0 = -3.317$, reaching a largest violation of -0.141 . Plot (b) shows a zoom on the moments of violation.

for an initial momentum state $|p\rangle$, which we will see below appears in the calculation of the quasi-probability.

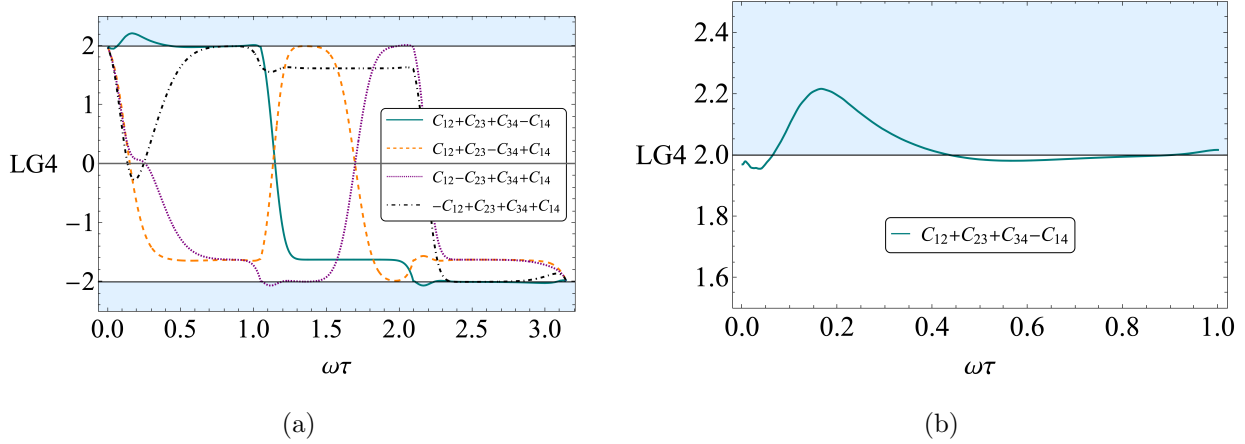


FIG. 5: Plot (a) shows the four LG4 inequalities, for state $x_0 = 0.929$, $p_0 = -3.666$, with largest violation reaching a largest violation of 2.216. Plot (b) shows a zoom of one of the inequalities.

A. Analysis with Currents

As we saw in Section. 3, the quasi-probability component $q(-, +)$ exhibits a healthy degree of negativity. We start by writing it as

$$q(-, +) = \int_0^\tau dt \frac{dq}{dt}. \quad (4.2)$$

It is then simple to relate $\frac{dq}{dt}$ to a set of quantum mechanical currents, which can be calculated analytically. Overall negativity of the QP can then be spotted by the non-classicality or negativity of certain combinations of currents.

We begin by writing the simple projector identity

$$P\rho + \rho P = P\rho P - \bar{P}\rho\bar{P} + \rho, \quad (4.3)$$

where $\bar{P} = 1 - P$. Hence the quasi-probability is given by

$$q(-, +) = \frac{1}{2} \text{Tr} (P_+(t_2) (P_-(t_1)\rho P_-(t_1) - P_+(t_1)\rho P_+(t_1) + \rho)). \quad (4.4)$$

This may be written in terms of the non-negative sequential measurement probabilities

$$p_{12}(s_1, s_2) = \text{Tr} (P_{s_2}(t_2)P_{s_1}(t_1)\rho P_{s_1}(t_1)), \quad (4.5)$$

in the form

$$q(-, +) = \frac{1}{2} (p_{12}(-, +) - p_{12}(+, +) + \langle P_+(t_2) \rangle). \quad (4.6)$$

It is now simple to take the derivative with respect to t_2 , noting that

$$\frac{d}{dt}\theta(\hat{x}(t)) = \frac{1}{2m} (\hat{p}(t)\delta(\hat{x}(t)) + \delta(\hat{x}(t))\hat{p}(t)) = \hat{J}(t), \quad (4.7)$$

yielding

$$\frac{dq(-, +)}{dt} = \frac{1}{2} \text{Tr} \left(\hat{J}(t) (P_-(t_1)\rho P_-(t_1) - P_+(t_1)\rho P_+(t_1) + \rho) \right). \quad (4.8)$$

We now introduce the ‘chopped current’

$$J_{\pm}(t) = \langle \psi | \theta(\pm \hat{x}) \hat{J}(t) \theta(\pm \hat{x}) | \psi \rangle. \quad (4.9)$$

The chopped currents are therefore the currents of the wave-functions $\langle x | e^{-iHt} \theta(\pm \hat{x}) | \psi \rangle$, and note the connection to the Moshinsky function when $|\psi\rangle$ is expanded in the momentum basis. We now rewrite $q(-, +)$ as

$$q(-, +) = \frac{1}{2} \int_{t_1}^{t_2} dt (J_-(t) - J_+(t) + J(t)), \quad (4.10)$$

where $J(t) = \langle \hat{J}(t) \rangle$ is the standard quantum-mechanical current at the origin, without any chopping. The usual current $J(t)$ for our gaussian state is given by

$$J(t) = \frac{\omega}{\sqrt{\pi}} p_t e^{-x_t^2}. \quad (4.11)$$

The chopped current contains the complexity of the influence of the earlier measurement, and are hence quite complicated and given in Appendix C. To understand the connection between the negativity of the quasi-probability Eq. (4.10) and the behaviour of the currents, it is very convenient to consider the analogous classical currents which are in general defined by

$$\mathbb{J}(t) = \int_{-\infty}^{\infty} dp \int_{-\infty}^{\infty} dx p(t) \delta(x(t)) w(x, p), \quad (4.12)$$

for a suitably chosen initial phase-space distribution $w(x, p)$. For the un-chopped current $\mathbb{J}(t)$ this is taken to be the Wigner function of the coherent state, $W(x, p, x_0, p_0)$ Eq.(B.1), which conveniently, is non-negative. For the chopped currents it is taken to be $\theta(\pm x)W(x, p, x_0, p_0)$. We then easily see that

$$J(t) = \mathbb{J}_-(t) + \mathbb{J}_+(t), \quad (4.13)$$

where $\mathbb{J}_{\pm}(t)$ are the classical analogs to the post-measurement currents, whose calculation and explicit expressions are found in Appendix B.

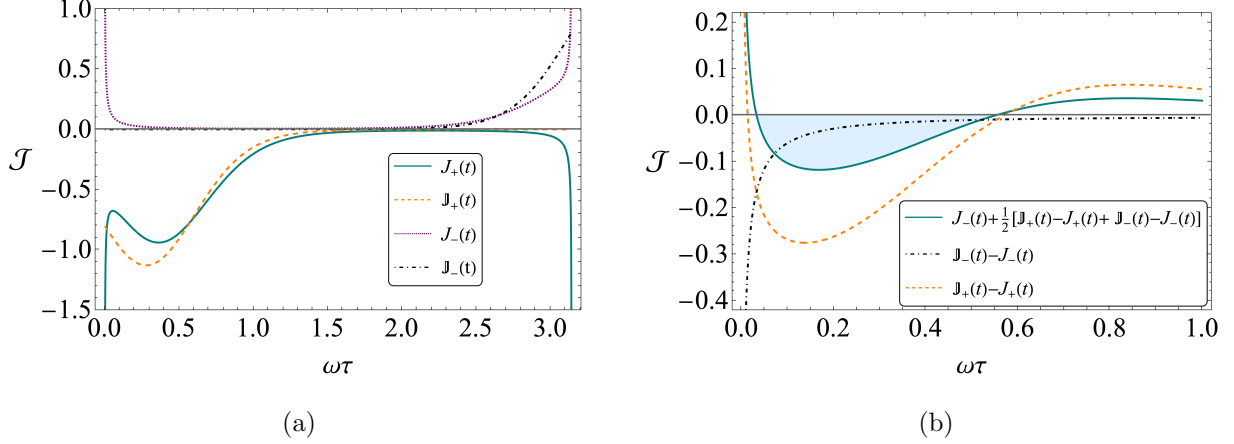


FIG. 6: Plot (a) shows the post-measurement quantum currents $J_{\pm}(t)$, and their classical analogs $\mathbb{J}_{\pm}(t)$, normalised to $\mathcal{J} = \frac{J}{\omega}$, for the coherent state with $x_0 = 0.55$, $p_0 = -1.925$. Plot (b) shows their combination appearing in the time derivative of $q(-, +)$, Eq. (4.14).

The quasi-probability is now readily rewritten as

$$q(-, +) = \int_{t_1}^{t_2} dt J_{-}(t) + \frac{1}{2} \int_{t_1}^{t_2} dt (\mathbb{J}_{-}(t) - J_{-}(t) + \mathbb{J}_{+}(t) - J_{+}(t)). \quad (4.14)$$

Note that the first time integral is simply the sequential measurement probability $p_{12}(-, +)$, which is non-negative. The negativity of the quasi-probability therefore arises as a result of the difference between the classical and quantum chopped currents.

The classical and quantum chopped currents and the current combination appearing in Eq. (4.10) are all plotted in Figure 6 for the initial state giving the LG2 violation described in Section 3. The departures from classicality are clearly seen and are consistent with a broadening of the momentum distribution produced by the measurement. Note also that the quantum chopped currents diverge initially due to the sharpness of the measurement.

Most importantly, we see that the combination of currents appearing in the quasi-probability Eq. (4.10) will clearly produce an overall negativity when integrated over time, thereby confirming the LG2 violation shown in Fig. 3. Furthermore, we have integrated Eq. (4.10) numerically and find an exact agreement with the calculation of Section 2, Eq. (2.16) thereby providing an independent check of this result.

It is also convenient to explore the currents in the small time limit which can be determined through use of a Taylor expansion, which may then be used to calculate the quasi-probability. This is done in Appendix D, where the calculation is applicable for general

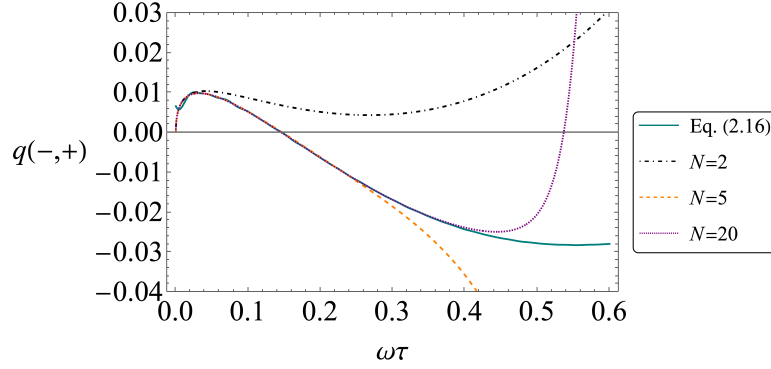


FIG. 7: The small-time expansion of $q(-, +)$ plotted alongside the previous calculation, at varying degrees of truncation, where $N = 2$ corresponds to Eq. (4.15).

$\psi(x)$. Taking just the first three terms of this expansion, we find

$$q(-, +) = \frac{1}{2\sqrt{\pi}} |\psi(0, 0)|^2 \tan^{\frac{1}{2}} \omega \tau + \frac{J(0)}{2} \tan \omega \tau + \frac{1}{6\sqrt{\pi}} \left(|\psi'(0, 0)|^2 - \left[\frac{1}{4} + \frac{3i}{4} \right] \psi'''(0, 0) \psi(0, 0) - \left[\frac{1}{4} - \frac{3i}{4} \right] \psi''(0, 0) \psi^*(0, 0) \right) \tan^{\frac{3}{2}} \omega \tau. \quad (4.15)$$

The initial divergence of the quantum chopped current is clearly seen. These results also agree with the small time expansion of chopped currents given by Sokolowski [33], giving another useful check on our calculations. For our gaussian initial state we find agreement with the results above, we plot this expansion alongside our original calculation in Fig.7. Furthermore, since these expressions are valid for any initial state they could provide a useful starting point in the search for other initial states giving LG2 violations larger than the somewhat modest violations found here.

B. Bohm trajectories

To give a visual demonstration of how the measurements influence motion in a way to lead to LG2 violations, we now calculate and plot the de Broglie-Bohm trajectories [34–36].

As noted earlier, the Moshinsky function underlies the behaviour of the quasi-probability for these measurements, so we initially examine the Bohm trajectories for this scenario. Using Moshinsky's calculation (free particle dynamics), we calculate the quantum-mechanical

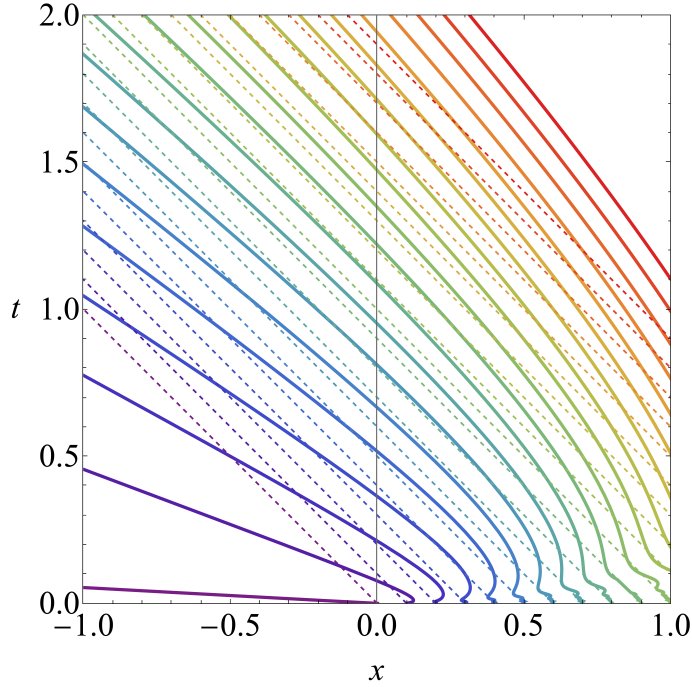


FIG. 8: The Bohm trajectories associated with the Moshinsky function, $\langle x|e^{-iHt}\theta(\hat{x})|p\rangle$ with $p = -1$. The equivalent classical paths are shown dotted.

current $J_M(x, t)$, which we then use in the guidance equation for Bohm trajectories,

$$\dot{x}(t) = \frac{J_M(x, t)}{|M(x, p, t)|^2}, \quad (4.16)$$

which we proceed to solve numerically.

In Fig. 8, we plot the trajectories for a state initially constrained to the right-hand side of the axis, with a left-ward momentum, with classical trajectories shown dotted.

From this we see two distinct phases of deviation from the classical result. Initially the trajectories rapidly exit the right hand side, with a negative momentum larger than in the classical case, an anti-Zeno effect [37]. After a short while, a Zeno effect [38, 39] happens, and the trajectories bend back relative to the classical trajectories, staying in the right hand side longer than in the classical case. We will see both of these behaviours at play in the case studied in this paper.

Using the expressions for the chopped current Eq. (C.18) and chopped wave-function Eq. (C.14), we can write the guidance equation for the harmonic oscillator case,

$$\dot{x}(t) = \frac{J_{\pm}(x, t)}{|\phi_{\alpha}^{\pm}(x, t)|^2}, \quad (4.17)$$

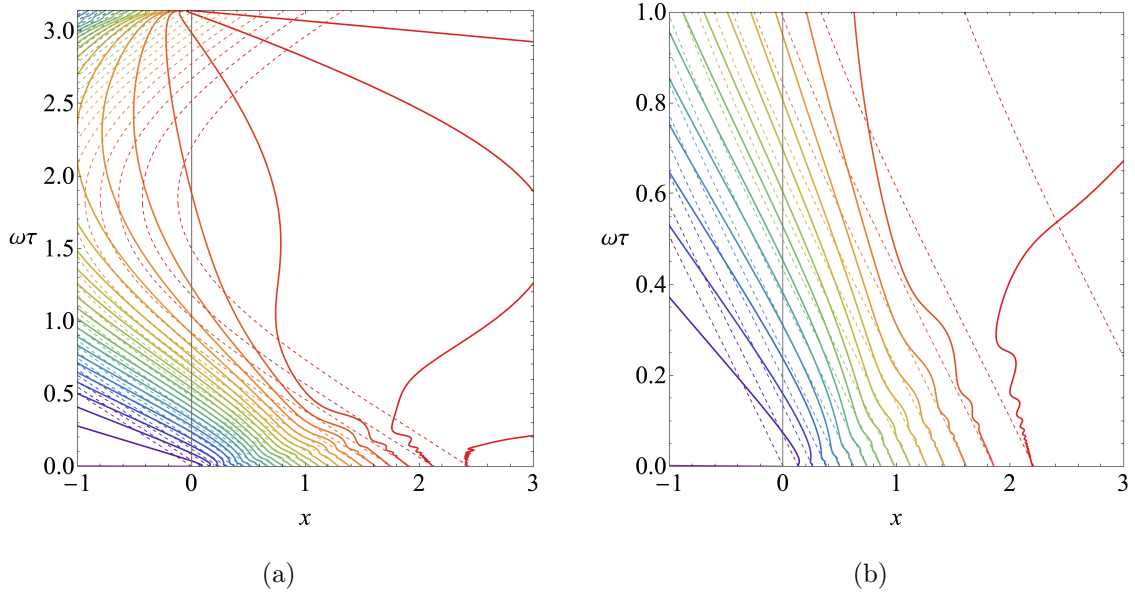


FIG. 9: The Bohm trajectories for case of the particle being initially found on the right hand side of the axis. In Fig (a), trajectories are separated such that two adjacent lines bound the evolution of 6.67% of the probability density, and in (b) they bound 10% of the probability density.

which we again solve numerically.

In Fig. 9, we show the Bohm trajectories for the state with $x_0 = 0.55$, $p_0 = -1.925$, initially found on the right hand side of the well. This corresponds to the behaviour of the current $J_+(x, t)$ from the previous section. Looking at the zoom of the trajectories in Fig. 9(b), we can observe the same behaviour that is seen in the Moshinsky case – initially an anti-Zeno effect, during which the trajectories exit faster than they would classically, followed by a Zeno effect a short while later, where trajectories exit more slowly than in the classical case.

This lines up with the behaviour of $\mathbb{J}_+(t) - J_+(t)$ displayed in Fig. 6(b), and is hence a representation on the trajectory level of the source of the LG2 violations.

5. WIGNER FUNCTION APPROACH

Another way to understand the LG2 violations, is within the Wigner representation. Since coherent states have non-negative Wigner functions, the source of MR violation lies in the non-gaussianity of the Wigner transform of the operators describing the measurement

procedure.

The Wigner-Weyl transform, which maps Hermitian operators to real phase space functions [40–43], is defined by

$$W_A(X, p) = \frac{1}{2\pi} \int_{-\infty}^{\infty} d\xi e^{-ip\xi} \langle X + \frac{\xi}{2} | A | X - \frac{\xi}{2} \rangle. \quad (5.1)$$

Traces of pairs of operators may be expressed in the Wigner representation as

$$\text{Tr}(\hat{A}\hat{B}) = 2\pi \int_{-\infty}^{\infty} dX \int_{-\infty}^{\infty} dp W_A(X, p) W_B(X, p). \quad (5.2)$$

To apply this formula to the quasi-probability there are two natural ways to proceed. First, in Ref. [28], the free particle quasi-probability was explored in Wigner-Weyl form using $\hat{A} = \frac{1}{2}(P_{s_1}P_{s_2} + P_{s_2}P_{s_1})$ and $\hat{B} = \rho$. However this was not found to be very useful since $W_A(X, p)$ in this case is highly oscillatory and it was not possible to clearly identify the regions of negativity, hence we proceed with a different approach.

We first write the QP in the form $q(s_1, s_2) = \text{Tr}(\bar{\rho}_{s_1}P_{s_2}(\tau))$, where $\bar{\rho}_{s_1} = \frac{1}{2}(P_{s_1}\rho + \rho P_{s_1})$, where $t_1 = 0$ without loss of generality. Hence by Eq. (5.2) we have

$$q(s_1, s_2) = 2\pi \int_{-\infty}^{\infty} dX \int_{-\infty}^{\infty} dp W_{\bar{\rho}_{s_1}}(X, p) W_{P_{s_2}(\tau)}(X, p), \quad (5.3)$$

where $W_{P_{s_2}}(X, p) = \theta(s_2(X \cos \omega t + p \sin \omega t))$. Using Eq. (5.1), the transform of $\bar{\rho}_{s_1}$ is given by

$$W_{\bar{\rho}_{s_1}}(X, p) = \frac{1}{4\pi} \int_{-\infty}^{\infty} d\xi e^{-ip\xi} \langle X + \frac{\xi}{2} | P_{s_1}\rho + \rho P_{s_1} | X - \frac{\xi}{2} \rangle, \quad (5.4)$$

which with details in Appendix E, is computed as

$$W_{\bar{\rho}_{s_1}}(X, p) = \frac{1}{2} W_{\rho}(X, p) (1 + \text{Re erf}(i(p - p_0) + s_1 X)), \quad (5.5)$$

in terms of $W_{\rho}(X, p)$, the Wigner function of the pure coherent state, given by

$$W_{\rho}(X, p) = \frac{1}{\pi} \exp(-(p - p_0)^2 - (X - x_0)^2). \quad (5.6)$$

The classical equivalent for Eq. (5.5) is $\frac{1}{2} W_{\rho}(X, p)(1 + \text{sgn}(x))$, which is approached for p close to p_0 and for large $|X|$.

The time evolution of the Wigner function in the case of the QHO is given by rigid rotation in accordance with classical paths $X_{\tau} = x_0 \cos \omega \tau - p_0 \sin \omega \tau$. Hence the final expression for the quasi-probability is given by

$$q(s_1, s_2) = \int_{-\infty}^{\infty} \int_{-\infty}^{\infty} dX dp \theta(s_2 X_{-\tau}) W_{\bar{\rho}_{s_1}}(X, p). \quad (5.7)$$

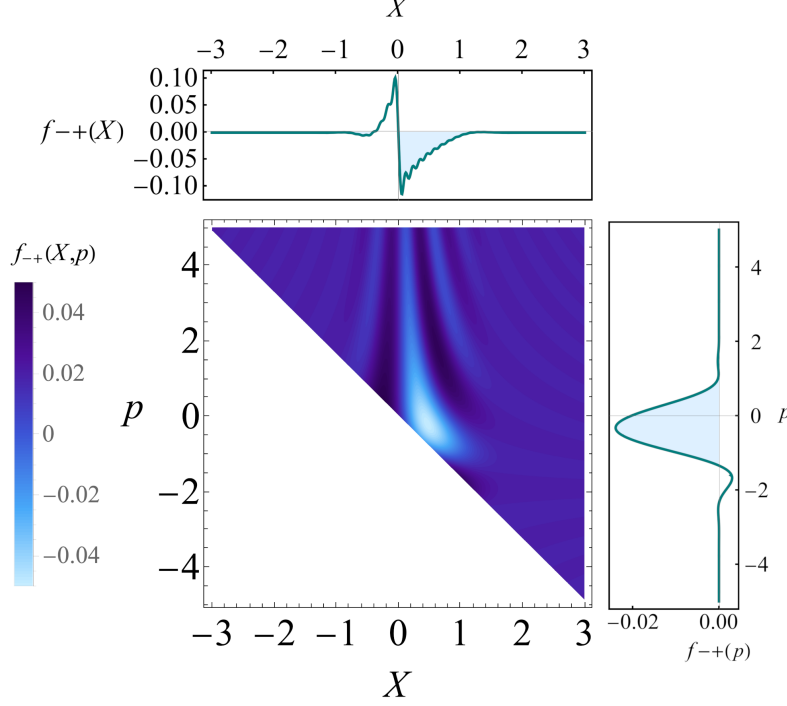


FIG. 10: We plot the phase-space density $f_{-,+}(X, p)$, in the case corresponding to an LG2 violation of -0.113 . Inset are the X and p marginals, shaded over regions of negativity.

We may hence write the quasi-probability as the integral

$$q(s_1, s_2) = \int_{-\infty}^{\infty} dX \int_{-\infty}^{\infty} dp f_{s_1, s_2}(X, p) \quad (5.8)$$

where the phase-space density $f_{s_1, s_2}(X, p)$ is given by

$$f_{s_1, s_2}(X, p) = \frac{1}{2} W_{\rho}(X, p) (1 + \text{Re erf}(i(p - p_0) + s_1 X)) \theta(s_2 X_{-\tau}) \quad (5.9)$$

In Fig. 10, we plot this phase-space density $f_{-,+}(X, p)$ for the state $x_0 = 0.55$, $p_0 = -1.925$ and $\omega\tau = 0.55$. To make it clear that this integrates to a negative number, we numerically determine the marginals $f_{-,+}(p) = \int_{-\infty}^{\infty} dX f_{-,+}(X, p)$ and likewise $f_{-,+}(X) = \int_{-\infty}^{\infty} dp f_{-,+}(X, p)$, plotting them as insets in Fig. 10. It is clear from a simple inspection of these marginals that they will integrate to a negative number.

In Appendix E, we plot the intermediate result Eq. (5.5), where it is apparent how the choice of second measurement hones in on the negativity introduced by the initial measurement, ultimately leading to the LG2 violations in Section 3.

6. OTHER TYPES OF MEASUREMENTS

It is useful to know what else may be possible beyond using $\theta(\hat{x})$ projectors. We note investigations [23] into smoothed $\theta(\hat{x})$ measurements, showing LG violations persist under smoothing of measurements up to the characteristic length-scale of the oscillator [22]. Modular variables such as $\cos(k\hat{x})$ have also been investigated, and readily produce significant LG violations [44]. These examples show that the LG violations are not due to the sharpness of projective measurements with $\theta(\hat{x})$.

In this section we will look at tests of macrorealism using coherent state projectors [45–47], which are interesting since they leave the post-measurement state gaussian, and are easily experimentally realised.

A. Coherent state projectors

We now consider coherent state projectors, where we have $P_+ = |\beta\rangle\langle\beta|$, and $P_- = \mathbb{1} - |\beta\rangle\langle\beta|$ defining a dichotomic variable in the usual way through Eq. (2.8). The quasi-probability is given by

$$q(+, +) = \text{Re} \langle \alpha | e^{iHt_2} |\beta_2\rangle\langle\beta_2| e^{-iH\tau} |\beta_1\rangle\langle\beta_1| e^{-iHt_1} | \alpha \rangle, \quad (6.1)$$

where we make two simplifying observations. Firstly, all the time evolution may be absorbed into the measurement projectors. Secondly, without loss of generality, we work with $\alpha = 0$, where the change in phase-space location may be absorbed into β_1 and β_2 . It is hence entirely equivalent to analyse

$$q(+, +) = \text{Re} \langle 0 | \gamma_1 \rangle \langle \gamma_1 | \gamma_2 \rangle \langle \gamma_2 | 0 \rangle, \quad (6.2)$$

with the relation $\gamma_i = e^{-i\omega t_i} \beta_i - \alpha$. The overlap between two coherent states is given by

$$\langle \beta | \alpha \rangle = e^{-\frac{1}{2}(|\alpha|^2 + |\beta|^2 - 2\alpha\beta^*)}, \quad (6.3)$$

and we readily find

$$q(+, +) = \exp(-|\gamma_1|^2 - |\gamma_2|^2) \text{Re} \exp(\gamma_1 \gamma_2^*), \quad (6.4)$$

$$q(+, -) = \exp(-|\gamma_1|^2) (1 - \text{Re} \exp(\gamma_1 \gamma_2^* - |\gamma_2|^2)), \quad (6.5)$$

where $q(-, +)$ is found by a relabelling, and $q(-, -)$ does not lead to any violations.

To determine the largest violations, it is useful to note these quasi-probabilities depend only on the magnitude of γ_1 and γ_2 , and the phase difference between them.

In $q(+, +)$, $|\gamma_1|$ and $|\gamma_2|$ appear in the same way, so we set them to be equal, and find a largest violation of -0.0133 at $\gamma_1 = 1.55$, $\gamma_2 = 1.55e^{-1.047i}$, which is about 10% of the maximal violation.

For $q(-, +)$, since the violation is aided by the negative sign on $\text{Re exp}(\gamma_1\gamma_2^* - |\gamma_2|^2)$, it is easy to see the largest violation will occur when both γ_1 and γ_2 are purely real. We readily find that the largest violation is approximately -0.1054 with $\gamma_2 = \frac{1}{2}\gamma_1 = 0.536$, which is about 84% of the maximum.

By writing the QP in the form given in Ref. [28]

$$q(s_1, s_2) = \frac{1}{8} \langle (1 + s_1\hat{Q}_1 + s_2\hat{Q}_2)^2 - 1 \rangle \quad (6.6)$$

we see that the maximally violating state satisfies the eigenvalue equation

$$(s_1\hat{Q}_1 + s_2\hat{Q}_2) |\psi\rangle = -|\psi\rangle. \quad (6.7)$$

The superposition state $|\psi\rangle = -|\beta\rangle_1 - |\beta\rangle_2$ is properly normalized and gives a maximal violation for $q(+, +)$ if the coherent states are chosen so that $\langle\beta_1|\beta_2\rangle = -\frac{1}{2}$. Similarly for $q(+, -)$, the state $|\psi\rangle = |\beta\rangle_1 - \sqrt{3}|\beta\rangle_2$ leads to a maximal violation if we choose $\langle\beta_1|\beta_2\rangle = \frac{\sqrt{3}}{2}$.

7. THERMAL AND SQUEEZED STATES

We now briefly look at the effects of using different states in LG tests in the QHO, namely squeezed states, and thermal coherent states.

A. Squeezed States

The squeezed coherent state may be written [48],

$$|\alpha, \zeta\rangle = D(\alpha)S(\zeta)|0\rangle. \quad (7.1)$$

While the squeezing operator $S(\zeta)$ does not commute with the displacement operator $D(\alpha)$, there is a simple braiding relation, allowing us to write

$$|\alpha, \zeta\rangle = S(\zeta)D(\beta)|0\rangle = S(\zeta)|\beta\rangle, \quad (7.2)$$

with β depending on both α and ζ . With the quasi-probability given by

$$q(+, +) = \text{Re} \langle \psi | \theta(\hat{x}) \theta(\hat{x}(t)) | \psi \rangle, \quad (7.3)$$

for $|\psi\rangle$ given by a squeezed coherent state. We can consider moving the $S(\zeta)$ in $|\psi\rangle$ onto each $\theta(\hat{x})$ function, resulting in $S^\dagger(\zeta)\theta(\hat{x})S(\zeta)$ twice. Since the squeezing operator has the action of a canonical transform, taking \hat{x} and \hat{p} into a linear combination of themselves, we have that

$$S^\dagger(\zeta)\theta(\hat{x})\theta(\hat{x}(t))S(\zeta) = \theta(a\hat{x} + b\hat{p})\theta(c\hat{x} + d), \quad (7.4)$$

for some a, b, c, d that may depend on t . We now note that $a\hat{x} + b\hat{p}$ may be written as $\lambda(\hat{x} \cos(t') + \hat{p} \sin(t'))$ for some $\lambda > 0$ and some t' , and since the theta-function is invariant under scaling, we see that

$$S^\dagger(\zeta)\theta(\hat{x})\theta(\hat{x}(t))S(\zeta) = \theta(\hat{x}(t'_1))\theta(\hat{x}(t'_2)). \quad (7.5)$$

This means the QP for a squeezed coherent state is equal to the QP for some other coherent state β , with different measurement times t'_1, t'_2 . Hence the operation of squeezing will not increase the largest possible violation reported in Section 3, although for certain states with sub-optimal violation, squeezing will increase the amount of violation.

B. Thermal States

The thermal coherent state at a temperature T is given by

$$\rho_{\text{th}}(\alpha, T) = \frac{1}{Z} \sum_{n=0}^{\infty} e^{-\frac{n\hbar\omega}{k_B T}} |n, \alpha\rangle\langle n, \alpha|, \quad (7.6)$$

where k_B is the Boltzmann constant, $|n, \alpha\rangle$ are energy eigenstates displaced by α in phase-space [49]. The partition function Z is given by

$$Z = \frac{1}{1 - e^{-\frac{\hbar\omega}{k_B T}}}. \quad (7.7)$$

Since this state is a mixture, it is simple to update the calculation Eq. (2.13) to using this state, leading to

$$q(+, -) = -\frac{1}{Z} \text{Re} \sum_{\ell=0}^{\infty} e^{-\frac{\ell\hbar\omega}{k_B T}} \sum_{n=0}^{\infty} e^{-i(n-\ell)\omega\tau} J_{\ell n}(x_1, \infty) J_{\ell n}(x_2, \infty) \quad (7.8)$$

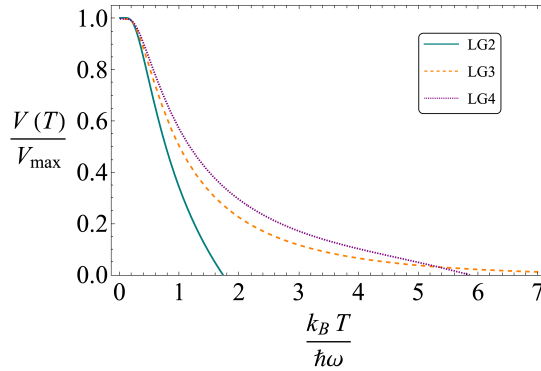


FIG. 11: The LG2, LG3 and LG4 violations are plotted as a fraction of their largest violation, for a state and time which realises V_{\max} , with varying temperature.

where the $J_{n\ell}$ matrices are given by Eq. (2.14), except for the cases $n = \ell$, where they must be calculated explicitly. A similar result may be calculated for the correlators using Eq. (2.17), allowing the analysis of LG3 and LG4 inequalities.

In Fig. 11 using the states found in Section 3, we plot the behaviour of the largest violation, as temperature is increased. We see the violation persists up to temperatures $k_B T \approx \hbar \omega$, with some preliminary evidence that LG3 and LG4 violations may be more robust against thermal fluctuations in the initial state.

8. SUMMARY

We have undertaken a study of LG violations in the quantum harmonic oscillator for a dichotomic variable $Q = \text{sgn}(x)$ and for an initial state given by a coherent state and closely related states. In Section 2, building on our earlier work with energy eigenstates of the QHO [22], we showed how the quasi-probability, and hence the temporal correlators, may be expressed as a discrete infinite sum which is amenable to numerical analysis. In Section 3 we applied this analysis to the LG2, LG3 and LG4 inequalities and carried out parameter space searches. We found LG violations of magnitude 22%, 28% and 26% of the maximum possible for the LG2, LG3 and LG4 inequalities, respectively, and gave the specific parameters for which these violations are achieved. These violations appear to be robust under small parameter adjustments.

The LG2 violation in the case $x_0 = 0$ agrees with that reported in Ref. [30]. The LG4

violation is significantly smaller than that reported in Ref. [23], which used a coherent state with large momentum. Our parameter search did not find any violations in this regime although the authors of Ref. [23] note that their violation arises only in a narrow parameter range.

In Section 4 we sought a physical understanding of the mechanism producing the violations. We showed how to relate the quasi-probability (LG2) to a set of currents for projected initial states. We calculated and plotted these currents and also plotted their associated Bohm trajectories along with their classical counterparts. The plots showed the clear departures from classicality and give both a visual understanding and independent check of the LG2 violations described in Section 3. We noted that the quantum effect producing the violations is essentially the diffraction in time effect first noted by Moshinsky [31, 32].

We explored the same issues from a different angle using the Wigner representation in Section 5. The Wigner function of the initial coherent state is everywhere non-negative. We determined and plotted the Wigner function of the chopped initial state appearing in the quasi-probability. It has significant regions of negativity which are clearly the source of the LG2 violation.

We briefly noted in Section 6 that our work is readily generalized from pure projective measurements to smoothed step function projectors, gaussian projectors and modular variables such as $\cos(\hat{x})$. We also examined the LG2 inequality for the case in which both projectors are taken to be projections onto coherent states. We showed that decent violations are possible for an initial coherent state and that a maximal violation arises when the initial state is a superposition of two coherent states.

In Section 7 we briefly discussed how the LG violations may be modified using families of states similar to a coherent state. We argued that squeezing the coherent state is unlikely to produce larger violations. We also considered a thermal initial state and estimated the degree to which thermal fluctuations may affect the degree of violation.

Acknowledgements

We are grateful to Sougato Bose, Dipankar Home, and Debarshi Das for useful discussions. We also thank Michael Vanner for discussions on the experimental feasibility of the tests discussed in this paper.

Appendix A: Separating quantum behaviour from classical trajectories

The two-time quasi-probability for a coherent state with a generic position basis measurement $m(\hat{x})$ is defined,

$$q(+, +) = \text{Re} \langle \alpha | e^{\frac{iHt_2}{\hbar}} m(\hat{x}) e^{-\frac{iH\tau}{\hbar}} m(\hat{x}) e^{-\frac{iHt_1}{\hbar}} | \alpha \rangle. \quad (\text{A.1})$$

We are primarily interested in the case $m(\hat{x}) = \theta(\hat{x})$, but what follows holds for more general $m(\hat{x})$, e.g gaussian measurements. Writing this in terms of the displacement operator, we have

$$q(+, +) = \text{Re} \langle 0 | D^\dagger(\alpha) e^{\frac{iHt_2}{\hbar}} m(\hat{x}) e^{-\frac{iH\tau}{\hbar}} m(\hat{x}) e^{-\frac{iHt_1}{\hbar}} D(\alpha) | 0 \rangle. \quad (\text{A.2})$$

Since the displacement operator is unitary, we have $D^\dagger(\alpha)D(\alpha) = \mathbb{1}$. Hence if we may commute the two displacement operators to be neighbours, we will clearly reach a vast simplification of the calculation.

To make the exposition clearer, we consider splitting this expression into two states

$$|M(\alpha, t_1, \tau)\rangle = e^{-i\hat{H}\tau} m(\hat{x}) e^{-\frac{iHt_1}{\hbar}} D(\alpha) | 0 \rangle, \quad (\text{A.3})$$

$$\langle M(\alpha, t_2, 0) | = \langle 0 | D^\dagger(\alpha) e^{\frac{iHt_2}{\hbar}} m(\hat{x}), \quad (\text{A.4})$$

where we then have $q(+, +) = \text{Re} \langle M(\alpha, t_2, 0) | M(\alpha, t_1, \tau) \rangle$, where we have introduced the notation $|M(\alpha, t, s)\rangle$ to represent the coherent state measured with $m(\hat{x})$ at time t , then evolved by time s .

Considering now the displacement operator acting to the left, we write $m(\hat{x})D(\alpha) = D(\alpha)D^\dagger(\alpha)m(\hat{x})D(\alpha) = D(\alpha)m(\hat{x} + x_\alpha)$, we have

$$|M(\alpha, t_1, \tau)\rangle = e^{-\frac{i\omega t_1}{2}} e^{-i\hat{H}\tau} D(\alpha(t_1)) m(\hat{x} + x_1) | 0 \rangle, \quad (\text{A.5})$$

Using the standard result that $e^{-iHt}D(\alpha)e^{iHt} = D(\alpha(t))$, we can rewrite this as

$$|M(\alpha, t_1, \tau)\rangle = e^{-\frac{i\omega t_1}{2}} D(\alpha(t_2)) e^{-iH\tau} m(\hat{x} + x_1) | 0 \rangle. \quad (\text{A.6})$$

This says that the post-measurement state is the evolution of the regular ground-state undergone a translated measurement, translated by the displacement operator, to a classical trajectory. Proceeding similarly with the other term, we find

$$\langle M(\alpha, t_2, 0) | = e^{\frac{i\omega t_2}{2}} \langle 0 | m(\hat{x} + x_2) D^\dagger(\alpha(t_2)). \quad (\text{A.7})$$

Finally, contracting the two terms we are able to exploit the unitarity of $D(\alpha)$ to find

$$q(+, +) = \text{Re } e^{\frac{i\omega\tau}{2}} \langle 0 | m(\hat{x} + x_2) e^{-iH\tau} m(\hat{x} + x_1) | 0 \rangle, \quad (\text{A.8})$$

Appendix B: Classical Analogs

To compare quantum mechanical behaviour to a classical mechanics, we calculate a classical analog of the post-measurement currents, as well as the quasi-probability, using phase-space methods. We begin by writing the classical phase-space density for the Gaussian state

$$\mathbb{W}(X, p, x_0, p_0) = \frac{1}{\pi} \exp(-(X - x_0)^2 - (p - p_0)^2), \quad (\text{B.1})$$

where harmonic time-evolution leads to rigid rotation in phase-space,

$$\mathbb{W}(X, p, x_0, p_0, t) = \mathbb{W}(X \cos \omega t - p \sin \omega t, p \cos \omega t + X \sin \omega t, x_0, p_0). \quad (\text{B.2})$$

We have a similar result for the measured classical state, with

$$\mathbb{W}_{\pm}(X, p, x_0, p_0) = \frac{1}{\pi} \theta(\pm X) \exp(-(X - x_0)^2 - (p - p_0)^2), \quad (\text{B.3})$$

and

$$\mathbb{W}_{\pm}(X, p, x_0, p_0, t) = \mathbb{W}_{\pm}(X \cos \omega t - p \sin \omega t, p \cos \omega t + X \sin \omega t, x_0, p_0). \quad (\text{B.4})$$

The chopped classical current is given by

$$\mathbb{J}_{\pm}(x, t) = \int_{-\infty}^{\infty} dp \int_{-\infty}^{\infty} dX p \delta(X - x) \mathbb{W}_{\pm}(X, p, x_0, p_0, t) \quad (\text{B.5})$$

Completing the X integral trivially, we have

$$\mathbb{J}_{\pm}(x, t) = \int_{-\infty}^{\infty} dp p \mathbb{W}_{\pm}(x, p, x_0, p_0, t). \quad (\text{B.6})$$

We are interested in the case of $x = 0$, which we shorthand $\mathbb{J}_{\pm}(0, t) = \mathbb{J}_{\pm}(t)$, and is given by

$$\mathbb{J}_{\pm}(t) = \frac{1}{\pi} \int_{-\infty}^{\infty} dp p \theta(\mp p \sin \omega t) \exp(-(p \cos \omega t - p_0)^2 - (-p \sin \omega t - x_0)^2). \quad (\text{B.7})$$

The step-function here just flips the integral between the positive or negative half-plane, dependent on $\text{sgn}(\mp \sin \omega t) = 1$ and $\text{sgn}(\mp \sin \omega t) = -1$ respectively. Computing the integral, this yields the result

$$\mathbb{J}_{\pm}(t) = \frac{1}{2\pi} e^{-p_0^2 - x_0^2} \left(\mp \text{sgn}(\sin \omega t) + \sqrt{\pi} e^{g(x_0, p_0, t)^2} g(x_0, p_0, t) (1 \mp \text{sgn}(\sin \omega t) \text{erf}(g(x_0, p_0, t))) \right), \quad (\text{B.8})$$

with $g(x_0, p_0, t) = p_0 \cos \omega t - x_0 \sin \omega t$.

Appendix C: Calculation of Currents

We calculate the ‘chopped current’ first, that is

$$J_{\pm}(x, t) = \frac{1}{2m} \langle \phi_{\alpha}^{\pm}(t) | \delta(\hat{x} - x) \hat{p} + \hat{p} \delta(\hat{x} - x) | \phi_{\alpha}^{\pm}(t) \rangle, \quad (\text{C.1})$$

where $\phi_{\alpha}^{\pm}(t)$ is the time evolution of a coherent state, initially projected on $\theta(\pm\hat{x})$ at t_0 ,

$$|\phi_{\alpha}^{\pm}(t)\rangle = e^{-iHt} \theta(\pm\hat{x}) |\alpha\rangle \quad (\text{C.2})$$

Calculating the current in the position basis, we have

$$J_{\pm}(x, t) = -\frac{i\hbar}{2m} \left(\phi_{\alpha}^{\pm*}(x, t) \frac{\partial \phi_{\alpha}^{\pm}(x, t)}{\partial x} - \frac{\partial \phi_{\alpha}^{\pm*}(x, t)}{\partial x} \phi_{\alpha}^{\pm}(x, t) \right), \quad (\text{C.3})$$

equivalent to

$$J_{\pm}(x, t) = \frac{\hbar}{m} \text{Im} \left(\phi_{\alpha}^{\pm*}(x, t) \frac{\partial \phi_{\alpha}^{\pm}(x, t)}{\partial x} \right). \quad (\text{C.4})$$

We calculate the evolved chopped state by

$$\phi_{\alpha}^{\pm}(x, t) = \int_{\Delta(\pm)} dy K(x, y, t) \psi_{\alpha}(y, t_0), \quad (\text{C.5})$$

where $\Delta(+) = [0, \infty)$, $\Delta(-) = (-\infty, 0]$,

$$\psi^{\alpha}(x, t_0) = \frac{1}{\pi^{\frac{1}{4}}} \exp \left(-\frac{1}{2}(x - x_0)^2 + ip_0 x \right). \quad (\text{C.6})$$

is the non-dimensionalized coherent state wave-function, with time evolution $\alpha(t) = e^{-i\omega t} \alpha(0)$, and

$$K(x, y, t) = \left(\frac{1}{2\pi i \sin \omega t} \right)^{\frac{1}{2}} \exp \left(-\frac{1}{2i \sin \omega t} ((x^2 + y^2) \cos \omega t - 2xy) \right), \quad (\text{C.7})$$

is the propagator for the harmonic potential.

Inserting the relevant expressions within Eq. (C.5) yields

$$\begin{aligned} \phi_{\alpha}^{\pm}(x, t) = \left(\frac{1}{2\pi i \sin \omega t} \right)^{\frac{1}{2}} \left(\frac{1}{\pi} \right)^{\frac{1}{4}} \int_{\Delta(\pm)} dy \exp \left(-\frac{1}{2}(y - x_0)^2 + iyp_0 \right) \times \\ \exp \left(-\frac{x^2 + y^2}{2i \tan \omega t} + \frac{xy}{i \sin \omega t} \right). \end{aligned} \quad (\text{C.8})$$

We proceed writing the integral as

$$I_{\pm}(a, b, c) = \int_{\Delta(\pm)} dr \exp \left(-\frac{1}{2}(r - a)^2 + ibr + icr^2 \right), \quad (\text{C.9})$$

where

$$a = x_0, \quad (C.10)$$

$$b = p_0 - \frac{x}{\sin \omega t}, \quad (C.11)$$

$$c = \frac{1}{2 \tan \omega t}. \quad (C.12)$$

Completing the integration, we have

$$I_{\pm}(a, b, c) = \frac{\sqrt{\pi} e^{-\frac{2a^2c+2ab+ib^2}{4c+2i}} \left(1 \pm \operatorname{erf} \left(\frac{a+ib}{\sqrt{2-4ic}}\right)\right)}{\sqrt{2-4ic}}. \quad (C.13)$$

We hence can write the chopped wave-function as

$$\phi_{\alpha}^{\pm}(x, t) = \left(\frac{1}{2\pi i \sin \omega t}\right)^{\frac{1}{2}} \left(\frac{1}{\pi}\right)^{\frac{1}{4}} e^{-\frac{x^2}{2i \tan \omega t}} I_{\pm} \left(x_0, p_0 - \frac{x}{\sin \omega t}, \frac{1}{2 \tan \omega t}\right). \quad (C.14)$$

Putting Eq.(C.4) into rescaled units as well, we have

$$J_{\pm}(x, t) = \omega \operatorname{Im} \left(\phi_{\alpha}^{\pm*}(x, t) \frac{\partial \phi_{\alpha}^{\pm}(x, t)}{\partial x} \right). \quad (C.15)$$

To take the derivative we note $I_{\pm}(a, b, c)$ depends on s only in its second argument, and so we define

$$K_{\pm}(a, b, c) = \frac{\partial b}{\partial s} \frac{\partial}{\partial b} I_{\pm}(a, b, c), \quad (C.16)$$

which explicitly yields

$$K_{\pm}(a, b, c) = \frac{-1}{\sin \omega t} \frac{e^{-\frac{a^2}{2}} \left(-\sqrt{2\pi}(a+ib) e^{\frac{(a+ib)^2}{2-4ic}} \left(1 \pm \operatorname{erf} \left(\frac{a+ib}{\sqrt{2-4ic}}\right)\right) \mp 2\sqrt{1-2ic} \right)}{2\sqrt{1-2ic}(2c+i)} \quad (C.17)$$

Altogether, this yields the current

$$J_{\pm}(x, t) = \frac{\omega}{2\pi^{\frac{3}{2}}} \operatorname{Im} \left(\frac{1}{|\sin \omega t|} I_{\pm} \left(x_0, -p_0 + \frac{x}{\sin \omega t}, -\frac{1}{2 \tan \omega t}\right) \times \left(\frac{ix}{\tan \omega t} I_{\pm} \left(x_0, p_0 - \frac{x}{\sin \omega t}, \frac{1}{2 \tan \omega t}\right) + K_{\pm} \left(x_0, p_0 - \frac{x}{\sin \omega t}, \frac{1}{2 \tan \omega t}\right) \right) \right). \quad (C.18)$$

We also calculate the current of the original unperturbed coherent state, in these same rescaled units. Since coherent states are eigenfunctions of the annihilation operator, with eigenvalue $\alpha(t)$, it follows that

$$\frac{\partial}{\partial x} \psi_{\alpha}(x, t) = \psi_{\alpha}(x, t) \left(\sqrt{2}\alpha(t) - x \right). \quad (C.19)$$

Hence the current is given by

$$J(x, t) = \frac{\omega}{\sqrt{\pi}} \text{Im} \left(e^{-(x-\sqrt{2} \text{Re} \alpha(t))^2} (\sqrt{2} \alpha(t) - x) \right), \quad (\text{C.20})$$

where taking the imaginary part, and using Eq. (2.2), we have

$$J(x, t) = \frac{\omega}{\sqrt{\pi}} p_t e^{-(x-x_t)^2}. \quad (\text{C.21})$$

Appendix D: Small Time Current Expansions

We are interested in a small time expansion of the chopped current $J_{\pm}(t)$, for any general state $|\psi\rangle$. We start by defining the chopped-evolved state,

$$|\psi^{\pm}(t)\rangle = e^{-iHt} \theta(\pm \hat{x}) |\psi\rangle. \quad (\text{D.1})$$

We now follow Appendix C up to Eq. (C.15) to calculate the current, however this time using the general $|\psi\rangle$ state, leading to

$$J_{\pm}(t) = \omega \text{Im} \left(\psi^{\pm*}(0, t) \frac{\partial \psi^{\pm}(0, t)}{\partial x} \right), \quad (\text{D.2})$$

with $|\psi\rangle$ represented in the non-dimensional position basis, i.e. $\langle x|\psi\rangle = \left(\frac{m\omega}{h}\right)^{\frac{1}{4}} \psi(x)$, with a normalised $\psi(x)$ which is purely a function of x .

Using the QHO propagator as in App. C up to Eq. (C.8), now with the $|\psi\rangle$ state, we have

$$\psi^{\pm}(x, t) = \left(\frac{1}{2\pi i \sin \omega t} \right)^{\frac{1}{2}} \int_{\Delta(\pm)} dy \psi(y, 0) \exp \left(-\frac{x^2 + y^2}{2i \tan \omega t} + \frac{xy}{i \sin \omega t} \right). \quad (\text{D.3})$$

We are interested in the current at $x = 0$ which means we only need $\psi(x)$ and its first derivative evaluated at $x = 0$, leaving

$$\psi^{\pm}(0, t) = \left(\frac{1}{2\pi i \sin \omega t} \right)^{\frac{1}{2}} \int_{\Delta(\pm)} dy \psi(y, 0) \exp \left(-\frac{y^2}{2i \tan \omega t} \right). \quad (\text{D.4})$$

We now argue that for small t the main contribution to the integral will come from near the boundary of the chop, and hence Taylor expand $\psi(y, 0)$ around $y = 0$. By using the parametrisation $y = z(\tan \omega t)^{\frac{1}{2}}$, we simplify the exponential part of the integrand.

$$\psi(y, 0) = \sum_{n=0}^{\infty} \frac{\psi^{(n)}(0, 0)}{n!} z^n (\tan \omega t)^{\frac{n}{2}}. \quad (\text{D.5})$$

Using this in Eq. (D.4), and using the substitution within the integral, we have

$$\psi^\pm(0, t) = \left(\frac{\tan \omega t}{2\pi i \sin \omega t} \right)^{\frac{1}{2}} \int_{\Delta(\pm)} dz \exp\left(-\frac{z^2}{2i}\right) \sum_{n=0}^{\infty} \frac{\psi^{(n)}(0, 0)}{n!} z^n (\tan \omega t)^{\frac{n}{2}} \quad (\text{D.6})$$

Interchanging the order of summation and integration, we have

$$\psi^\pm(0, t) = \left(\frac{1}{2\pi i \cos \omega t} \right)^{\frac{1}{2}} \sum_{n=0}^{\infty} \frac{\psi^{(n)}(0, 0)}{n!} (\tan \omega t)^{\frac{n}{2}} \int_{\Delta(\pm)} dz e^{-\frac{z^2}{2i}} z^n. \quad (\text{D.7})$$

We now define

$$K_\pm(n) = \int_{\Delta(\pm)} dz e^{-\frac{z^2}{2i}} z^n, \quad (\text{D.8})$$

which can be calculated by taking the Fourier transform of $e^{iz^2}\theta(\pm z)$, taking n derivatives in Fourier space, and then evaluating with the conjugate variable set to 0, to give the result

$$K_\pm(n) = (\pm 1)^n 2^{\frac{n}{2}} e^{\frac{1}{4}i\pi(n+1)} \Gamma\left(\frac{n+1}{2}\right), \quad (\text{D.9})$$

where Γ is the Gamma function. This gives a final result of

$$\psi^\pm(0, t) = \left(\frac{1}{2\pi i \cos \omega t} \right)^{\frac{1}{2}} \sum_{n=0}^{\infty} K_\pm(n) \frac{\psi^{(n)}(0, 0)}{n!} (\tan \omega t)^{\frac{n}{2}}. \quad (\text{D.10})$$

We now calculate the derivative of the chopped wavefunction, by taking the derivative of Eq. (D.3), evaluated at $x = 0$ to find

$$\left. \frac{\partial \psi^\pm(x, t)}{\partial x} \right|_{x=0} = \frac{-i}{\sin \omega t} \left(\frac{1}{2\pi i \sin \omega t} \right)^{\frac{1}{2}} \int_{\Delta(\pm)} dy \psi(y, 0) y \exp\left(-\frac{y^2}{2i \tan \omega t}\right). \quad (\text{D.11})$$

We now note, that with the exception of the pre-factor $\frac{-i}{\sin \omega t}$, this is the same result as before, only with $\psi(y, 0)$ swapped for $y\psi(y, 0)$, leading to the result

$$\frac{\partial \psi^\pm(0, t)}{\partial x} = - \left(\frac{-1}{2\pi i \sin^2 \omega t \cos \omega t} \right)^{\frac{1}{2}} \sum_{n=0}^{\infty} K_\pm(n) \frac{\frac{\partial^n}{\partial y^n} (y\psi(y, 0))|_{y=0}}{n!} (\tan \omega t)^{\frac{n}{2}}. \quad (\text{D.12})$$

Then since

$$\left. \frac{\partial^n}{\partial y^n} y\psi(y, 0) \right|_{y=0} = n\psi^{(n-1)}(0, 0), \quad (\text{D.13})$$

we have as a final result

$$\frac{\partial \psi^\pm(0, t)}{\partial x} = - \left(\frac{-1}{2\pi i \sin^2 \omega t \cos \omega t} \right)^{\frac{1}{2}} \sum_{n=1}^{\infty} K_\pm(n) \frac{n\psi^{(n-1)}(0, 0)}{n!} (\tan \omega t)^{\frac{n}{2}}, \quad (\text{D.14})$$

noting the change on the sum's lower limit.

We now combine Eq. (D.10) and Eq. (D.14) to yield the small-time expansion for the chopped current

$$J_{\pm}(t) = \frac{-\omega}{2\pi \sin \omega t \cos \omega t} \text{Im} \left(i \sum_{\ell=0}^{\infty} \sum_{n=1}^{\infty} K_{\pm}(n) K_{\pm}^*(\ell) \frac{n\psi^{(n-1)}(0,0)\psi^{*(\ell)}(0,0)}{n!\ell!} (\tan \omega t)^{\frac{n+\ell}{2}} \right) \quad (\text{D.15})$$

We note that this result is in fact trivial to integrate over time by noting the derivative of $\tan(\omega t)$, yielding

$$\int_0^{\tau} dt \frac{(\tan \omega t)^{\frac{k}{2}}}{\sin \omega t \cos \omega t} = \frac{2}{k\omega} (\tan \omega \tau)^{\frac{k}{2}}. \quad (\text{D.16})$$

The time-integral of the chopped current is thus

$$\int_0^{\omega\tau} J_{\pm}(t) dt = -\frac{1}{\pi} \text{Im} \left(i \sum_{\ell=0}^{\infty} \sum_{n=1}^{\infty} K_{\pm}(n) K_{\pm}^*(\ell) \frac{n\psi^{(n-1)}(0,0)\psi^{*(\ell)}(0,0)}{(n+\ell)n!\ell!} (\tan \omega t)^{\frac{n+\ell}{2}} \right) \quad (\text{D.17})$$

We also note that by defining

$$L(n) = K_+(n) + K_-(n), \quad (\text{D.18})$$

we may adapt the result to the unchopped current as

$$J(t) = -\frac{\omega}{2\pi \sin \omega t \cos \omega t} \text{Im} \left(i \sum_{\ell=0}^{\infty} \sum_{n=1}^{\infty} L(n) L^*(\ell) \frac{n\psi^{(n-1)}(0,0)\psi^{*(\ell)}(0,0)}{n!\ell!} (\tan \omega t)^{\frac{n+\ell}{2}} \right), \quad (\text{D.19})$$

with time-integral

$$\int_0^{\omega\tau} J(t) dt = -\frac{1}{\pi} \text{Im} \left(i \sum_{\ell=0}^{\infty} \sum_{n=1}^{\infty} L(n) L^*(\ell) \frac{n\psi^{(n-1)}(0,0)\psi^{*(\ell)}(0,0)}{(n+\ell)n!\ell!} (\tan \omega t)^{\frac{n+\ell}{2}} \right) \quad (\text{D.20})$$

Using Eq. (4.10) to express the quasi-probability as the time integral of currents, and noting the similarity of the summands, we can write the quasi-probability for as

$$q(-, +) = -\frac{1}{2\pi} \text{Im} \left(i \sum_{\ell=0}^{\infty} \sum_{n=1}^{\infty} \mathcal{Q}(n, \ell) \frac{n\psi^{(n-1)}(0,0)\psi^{*(\ell)}(0,0)}{(n+\ell)n!\ell!} (\tan \omega t)^{\frac{n+\ell}{2}} \right), \quad (\text{D.21})$$

where

$$\mathcal{Q}(n, \ell) = K_-(n) K_-^*(\ell) - K_+(n) K_+^*(\ell) + L_n L_{\ell}^*. \quad (\text{D.22})$$

By approximating the infinite sums to finite order, we are able to approximate the quasi-probability. To get the first three terms of the approximation, we limit both sums to $\ell_{\max} = 2$

and $n_{max} = 3$, yielding

$$q(-, +) = \frac{1}{2\sqrt{\pi}} |\psi(0, 0)|^2 \tan^{\frac{1}{2}} \omega \tau + \frac{J(0)}{2} \tan \omega \tau + \frac{1}{6\sqrt{\pi}} \left(|\psi'(0, 0)|^2 - \left[\frac{1}{4} + \frac{3i}{4} \right] \psi''^*(0, 0) \psi(0, 0) - \left[\frac{1}{4} - \frac{3i}{4} \right] \psi''(0, 0) \psi^*(0, 0) \right) \tan^{\frac{3}{2}} \omega t + \mathcal{O}(\tan^2 \omega t) \quad (\text{D.23})$$

Taking the taking the $\omega \rightarrow 0$ expansions of the trigonometric terms recovers the result for the free particle,

$$q(-, +) = \frac{1}{2\sqrt{\pi}} |\psi(0, 0)|^2 \tau^{\frac{1}{2}} + \frac{J(0)}{2} \tau + \frac{1}{6\sqrt{\pi}} \left(|\psi'(0, 0)|^2 - \left[\frac{1}{4} + \frac{3i}{4} \right] \psi''^*(0, 0) \psi(0, 0) - \left[\frac{1}{4} - \frac{3i}{4} \right] \psi''(0, 0) \psi^*(0, 0) \right) \tau^{\frac{3}{2}}, \quad (\text{D.24})$$

which we note has a term in $\tau^{\frac{1}{2}}$ which was missing from an earlier calculation of this expansion in Ref. [28], as well as a different coefficient on the $\tau^{\frac{3}{2}}$ term.

Appendix E: Wigner Function calculational details

We without loss of generality we take $t_1 = 0$, and so $P_{s_1} = \theta(s_1 \hat{x})$, leading to

$$W_{\bar{\rho}_{s_1}}(X, p) = \frac{1}{4\pi} \int_{-\infty}^{\infty} d\xi e^{-ip\xi} \left(\theta(s_1(X + \frac{\xi}{2})) + \theta(s_1(X - \frac{\xi}{2})) \right) \langle X + \frac{\xi}{2} | \rho | X - \frac{\xi}{2} \rangle. \quad (\text{E.1})$$

Since coherent states are pure states, we have simply that $\rho(x, y) = \psi(x)\psi^*(y)$, where we will use natural units with $\psi(x) = \frac{1}{\pi^{\frac{1}{4}}} \exp(-\frac{1}{2}(x - x_0)^2 + ip_0 x)$. This yields the integrand as $I(X, \xi) = e^{-ip\xi} \exp\left(ip_0\xi - X^2 + 2Xx_0 - x_0^2 - \frac{\xi^2}{4}\right)$.

Demonstrating with the $s_1 = +1$ case, the theta functions are handled by splitting the integral into two integrals over the regions $[-2X, \infty)$, and $(-\infty, 2X]$, and so we have

$$W_{\bar{\rho}_{s_1}}(X, p) = \frac{1}{4\pi\sqrt{\pi}} \left(\int_{-2X}^{\infty} d\xi I(X, \xi) + \int_{-\infty}^{2X} d\xi I(X, \xi) \right), \quad (\text{E.2})$$

Computing the integral involved, we reach the result

$$W_{\bar{\rho}_{s_1}}(X, p) = \frac{1}{2\pi} e^{-(p-p_0)^2 - (X-x_0)^2} (1 + \text{Re erf}(i(p - p_0) + s_1 X)), \quad (\text{E.3})$$

which may be written in terms of the Wigner function of the coherent state $W_{\rho}(X, p)$ as

$$W_{\bar{\rho}_{s_1}}(X, p) = \frac{1}{2} W_{\rho}(X, p) (1 + \text{Re erf}(i(p - p_0) + s_1 X)). \quad (\text{E.4})$$

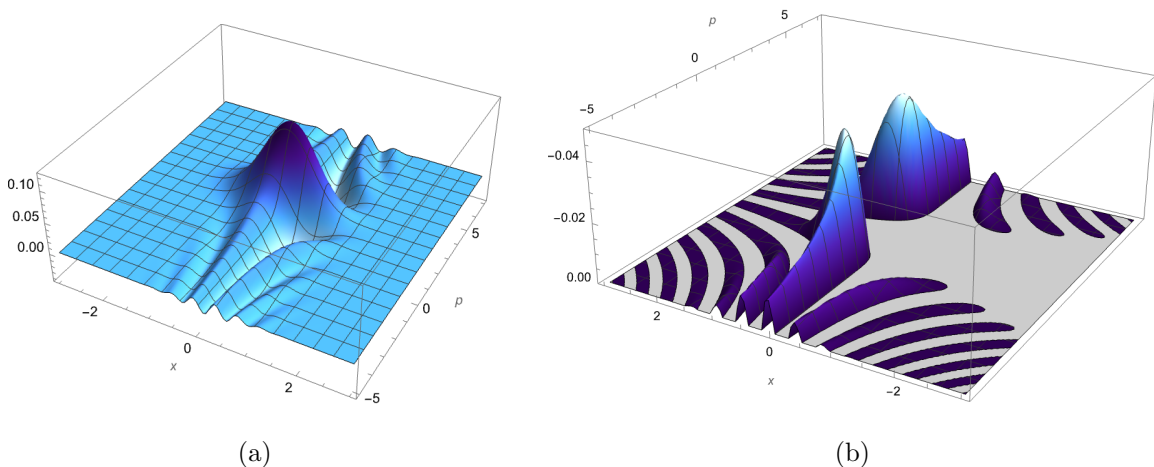


FIG. 12: Plot (a) shows $W_{\hat{\rho}_-}(x, p)$ for an initial coherent state with $x_0 = 0.55, p_0 = -1.925$ and $\omega\tau = 0.55$, with (b) (flipped axis) showing just the regions where the function is negative.

We plot $W_{\hat{\rho}_{s_1}}$ for a coherent state with the largest LG2 violation $x_0 = 0.550, p_0 = -1.925$ in Fig. 12(a), with just the negative parts isolated in Fig. 12(b). This indicates the negativity introduced in phase-space by the measurement. In the main text, Fig. 10, we see that the choice of time parameter of the second measurement selects one of the lobes of negativity in Fig. 12(b), while rejecting the main lobe of positivity seen in Fig. 12(a), such that the integral across phase-space is negative.

-
- [1] A. J. Leggett and Anupam Garg. Quantum mechanics versus macroscopic realism: Is the flux there when nobody looks? *Physical Review Letters*, 54(9):857–860, March 1985.
 - [2] A. J. Leggett. Experimental approaches to the quantum measurement paradox. *Foundations of Physics*, 18(9):939–952, September 1988.
 - [3] A. J. Leggett. Realism and the physical world. *Reports on Progress in Physics*, 71(2):022001, January 2008.
 - [4] Clive Emary, Neill Lambert, and Franco Nori. Leggett–Garg inequalities. *Reports on Progress in Physics*, 77(1):016001, December 2013.
 - [5] George C. Knee, Stephanie Simmons, Erik M. Gauger, John J. L. Morton, Helge Riemann, Nikolai V. Abrosimov, Peter Becker, Hans-Joachim Pohl, Kohei M. Itoh, Mike L. W. Thewalt, G. Andrew D. Briggs, and Simon C. Benjamin. Violation of a Leggett–Garg inequality with

- ideal non-invasive measurements. *Nature Communications*, 3(1):606, January 2012.
- [6] Carsten Robens, Wolfgang Alt, Dieter Meschede, Clive Emary, and Andrea Alberti. Ideal Negative Measurements in Quantum Walks Disprove Theories Based on Classical Trajectories. *Physical Review X*, 5(1):011003, January 2015.
 - [7] Hemant Katiyar, Aharon Brodutch, Dawei Lu, and Raymond Laflamme. Experimental violation of the Leggett–Garg inequality in a three-level system. *New Journal of Physics*, 19(2):023033, February 2017.
 - [8] J. J. Halliwell. Leggett-Garg correlation functions from a noninvasive velocity measurement continuous in time. *Physical Review A*, 94(5):052114, November 2016.
 - [9] Shayan-Shawn Majidy, Hemant Katiyar, Galit Anikeeva, Jonathan Halliwell, and Raymond Laflamme. Exploration of an augmented set of Leggett-Garg inequalities using a noninvasive continuous-in-time velocity measurement. *Physical Review A*, 100(4):042325, October 2019.
 - [10] Shayan-Shawn Majidy. Violation of an augmented set of Leggett-Garg inequalities and the implementation of a continuous in time velocity measurement. Master’s thesis, University of Waterloo, 2019.
 - [11] J. J. Halliwell. Leggett-Garg inequalities and no-signaling in time: A quasiprobability approach. *Physical Review A*, 93(2):022123, February 2016.
 - [12] J. J. Halliwell. Comparing Conditions for Macrorealism: Leggett-Garg Inequalities vs No-Signaling in Time. *Physical Review A*, 96(1):012121, July 2017.
 - [13] J. J. Halliwell. Necessary and sufficient conditions for macrorealism using two and three-time Leggett-Garg inequalities. *Journal of Physics: Conference Series*, 1275:012008, September 2019.
 - [14] J. J. Halliwell and C. Mawby. Fine’s theorem for Leggett-Garg tests with an arbitrary number of measurement times. *Physical Review A*, 100(4):042103, October 2019.
 - [15] J. J. Halliwell and C. Mawby. Conditions for macrorealism for systems described by many-valued variables. *Physical Review A*, 102(1):012209, July 2020.
 - [16] Mateus Araújo, Marco Túlio Quintino, Costantino Budroni, Marcelo Terra Cunha, and Adán Cabello. All noncontextuality inequalities for the n -cycle scenario. *Physical Review A*, 88(2):022118, August 2013.
 - [17] M. E. Goggin, M. P. Almeida, M. Barbieri, B. P. Lanyon, J. L. O’Brien, A. G. White, and G. J. Pryde. Violation of the Leggett–Garg inequality with weak measurements of photons.

- Proceedings of the National Academy of Sciences*, 108(4):1256–1261, January 2011.
- [18] J. A. Formaggio, D. I. Kaiser, M. M. Murskyj, and T. E. Weiss. Violation of the Leggett-Garg Inequality in Neutrino Oscillations. *Physical Review Letters*, 117(5):050402, July 2016.
 - [19] Kaushik Joarder, Debashis Saha, Dipankar Home, and Urbasi Sinha. Loophole-Free Interferometric Test of Macrorealism Using Heralded Single Photons. *PRX Quantum*, 3(1):010307, January 2022.
 - [20] George C. Knee, Kosuke Kakuyanagi, Mao-Chuang Yeh, Yuichiro Matsuzaki, Hiraku Toida, Hiroshi Yamaguchi, Shiro Saito, Anthony J. Leggett, and William J. Munro. A strict experimental test of macroscopic realism in a superconducting flux qubit. *Nature Communications*, 7(1):13253, November 2016.
 - [21] Owen J. E. Maroney and Christopher G. Timpson. Quantum- vs. Macro- Realism: What does the Leggett-Garg Inequality actually test? *arXiv:1412.6139 [quant-ph]*, December 2014.
 - [22] C. Mawby and J. J. Halliwell. Leggett-Garg tests for macrorealism in the quantum harmonic oscillator and more general bound systems. *Physical Review A*, 105(2):022221, February 2022.
 - [23] S Bose, D Home, and S Mal. Nonclassicality of the Harmonic-Oscillator Coherent State Persisting up to the Macroscopic Domain. *Physical Review Letters*, 120(21):210402, 2018.
 - [24] Debarshi Das, Dipankar Home, Hendrik Ulbricht, and Sougato Bose. Mass-independent test of quantumness of a massive object. *in preparation*, 2022.
 - [25] Johannes Kofler and Āaslav Brukner. Condition for macroscopic realism beyond the Leggett-Garg inequalities. *Physical Review A*, 87(5):052115, May 2013.
 - [26] Lucas Clemente and Johannes Kofler. Necessary and sufficient conditions for macroscopic realism from quantum mechanics. *Physical Review A*, 91(6):062103, June 2015.
 - [27] Lucas Clemente and Johannes Kofler. No Fine Theorem for Macrorealism: Limitations of the Leggett-Garg Inequality. *Physical Review Letters*, 116(15):150401, April 2016.
 - [28] J. J. Halliwell, H. Beck, B. K. B. Lee, and S. O’Brien. Quasiprobability for the arrival-time problem with links to backflow and the Leggett-Garg inequalities. *Physical Review A*, 99(1):012124, January 2019.
 - [29] M. Moriconi. Nodes of wavefunctions. *American Journal of Physics*, 75(3):284–285, March 2007.
 - [30] J. J. Halliwell, A. Bhatnagar, E. Ireland, H. Nadeem, and V. Wimalaweera. Leggett-Garg tests for macrorealism: Interference experiments and the simple harmonic oscillator. *Physical*

- Review A*, 103(3):032218, March 2021.
- [31] Marcos Moshinsky. Diffraction in Time. *Physical Review*, 88(3):625–631, November 1952.
 - [32] M. Moshinsky. Diffraction in time and the time–energy uncertainty relation. *American Journal of Physics*, 44(11):1037–1042, November 1976.
 - [33] D. Sokolovski. Schrodinger current for discontinuous states from the first-passage-time decomposition. *Physical Review A*, 86(1):012105, July 2012.
 - [34] David Bohm. A Suggested Interpretation of the Quantum Theory in Terms of “Hidden” Variables. I. *Physical Review*, 85(2):166–179, January 1952.
 - [35] David Bohm. A Suggested Interpretation of the Quantum Theory in Terms of “Hidden” Variables. II. *Physical Review*, 85(2):180–193, January 1952.
 - [36] Louis de Broglie. La mécanique ondulatoire et la structure atomique de la matière et du rayonnement. *J. Phys. Radium*, 8(5):225–241, 1927.
 - [37] B. Kaulakys and V. Gontis. Quantum anti-Zeno effect. *Physical Review A*, 56(2):1131–1137, August 1997.
 - [38] Alan Turing, R. O. Gandy, and C. E. M. Yates. *Mathematical Logic*. Collected Works of A. M. Turing. Elsevier Science, Amsterdam ; New York, 2001.
 - [39] B. Misra and E. C. G. Sudarshan. The Zeno’s paradox in quantum theory. *Journal of Mathematical Physics*, 18(4):756–763, April 1977.
 - [40] M. Hillery, R. F. O’Connell, M. O. Scully, and E. P. Wigner. Distribution functions in physics: Fundamentals. *Physics Reports*, 106(3):121–167, April 1984.
 - [41] V. I. Tatarskiĭ. The Wigner representation of quantum mechanics. *Soviet Physics Uspekhi*, 26(4):311, 1983.
 - [42] William B. Case. Wigner functions and Weyl transforms for pedestrians. *American Journal of Physics*, 76(10):937–946, October 2008.
 - [43] J. J. Halliwell. Quantum-mechanical histories and the uncertainty principle: Information-theoretic inequalities. *Physical Review D*, 48(6):2739–2752, September 1993.
 - [44] A. Asadian, C. Brukner, and P. Rabl. Probing Macroscopic Realism via Ramsey Correlation Measurements. *Physical Review Letters*, 112(19):190402, May 2014.
 - [45] Horace P. Yuen and Jeffrey H. Shapiro. Optical Communication with Two-Photon Coherent States—Part I: Quantum-State Propagation and Quantum-Noise Reduction. *IRE Professional Group on Information Theory*, 24(6):657–668, November 1978.

- [46] Horace P. Yuen and Vincent W. S. Chan. Noise in homodyne and heterodyne detection. *Optics Letters*, 8(3):177–179, March 1983.
- [47] G. Mauro D’Ariano, Matteo G. A. Paris, and Massimiliano F. Sacchi. Quantum Tomography. *Advances in Imaging and Electron Physics*, 128:205–308, February 2003.
- [48] Wolfgang Schleich. *Quantum Optics in Phase Space*. Wiley-VCH, Berlin ; New York, 2001.
- [49] J. Oz-Vogt, A. Mann, and M. Revzen. Thermal Coherent States and Thermal Squeezed States. *Journal of Modern Optics*, 38(12):2339–2347, December 1991.